



Review

An original method for characterizing internal waves

Gaëlle Casagrande^{a,*}, Alex Warn Varnas^b, Thomas Folégot^c, Yann Stéphan^a^aService Hydrographique et Océanographique de la Marine, 13 rue Le Chatellier, 29200 Brest, France^bNaval Research Laboratory, Stennis Space Centre, MS 39529, USA^cNATO Undersea Research Centre, Viale San Bartolomeo 400, 19126 La Spezia, Italy

ARTICLE INFO

Article history:

Received 19 December 2008

Received in revised form 29 July 2009

Accepted 30 July 2009

Available online 8 August 2009

Keywords:

Internal solitary waves

Empirical orthogonal function analysis

Changing rates

Double oscillation

Scatter diagram

Thermistor chain data

Italy

Sicily

Strait of Messina

ABSTRACT

This study consisted in the characterization of internal waves in the south of the Strait of Messina (Italy). The observational data consisted in thermistor string profiles from the Coastal Ocean Acoustic Changes at High frequencies (COACH06) sea trial.

An empirical orthogonal function analysis is applied to the data. The first two spatial empirical modes represent over 99% of the variability, and their corresponding time-dependent expansion coefficients take higher absolute values during internal wave events. In order to check how the expansion coefficients vary during an internal wave event, their time derivative, called here *changing rates*, are computed. It shows that each wave of an internal wave train is characterized by a double oscillation of the changing rates. At the front of the wave, both changing rates increase in absolute value with opposite sign, and then decrease to become null at the maximum amplitude of the wave. At the rear of the wave, the changing rates describe another period, again with opposite sign. This double oscillation can be used as a detector of internal waves, but it can also give information on the width of the wave, by measuring the length of the oscillation, as this information may sometimes be hard to read straight out of the data. When plotting the changing rates one versus another, the resulting scatter diagram puts on a butterfly shape that illustrates well this behaviour.

© 2009 Elsevier Ltd. All rights reserved.

Contents

1. Introduction	1
2. Experimental data	2
3. EOF analysis	3
4. Results	5
5. Summary and conclusions	7
Acknowledgments	8
References	8

1. Introduction

The Strait of Messina separates the Italian Peninsula from the island of Sicily. It is a natural connection between the Tyrrhenian Sea in the north and the Ionian Sea in the south. Consequently two water masses are encountered in the strait, the Tyrrhenian surface water and the colder and saltier Levantine Intermediate Water,

making it a rich dynamical area where many ocean features can be encountered. The strait is 3 km wide and 80 m deep at the sill. In the northern basin, the water depth increases gently whereas the slope is steeper in the southern basin (Fig. 1). During maximum tidal flow from the Tyrrhenian Sea to the Ionian Sea (*rema scendente*) and inversely (*rema montante*), only one type of water is present over the sill, thus annihilating the two-layer structure usually encountered over the sill: the tidal barotropic aspect of water motion was analyzed by Defant (1961). Although tidal sea surface displacements are very small in the strait of Messina (the order of 10 cm), Defant (1940) explained the existence of strong currents in the strait by the fact that the tides for the open strait boundaries

* Corresponding author. Tel.: +33 2 98 37 77 59; fax: +33 2 98 22 18 64.

E-mail addresses: gaelle.casagrande@shom.fr (G. Casagrande), varnas@nrlssc.navy.mil (A.W. Varnas), folegot@nurc.nato.int (T. Folégot), yann.stephan@shom.fr (Y. Stéphan).

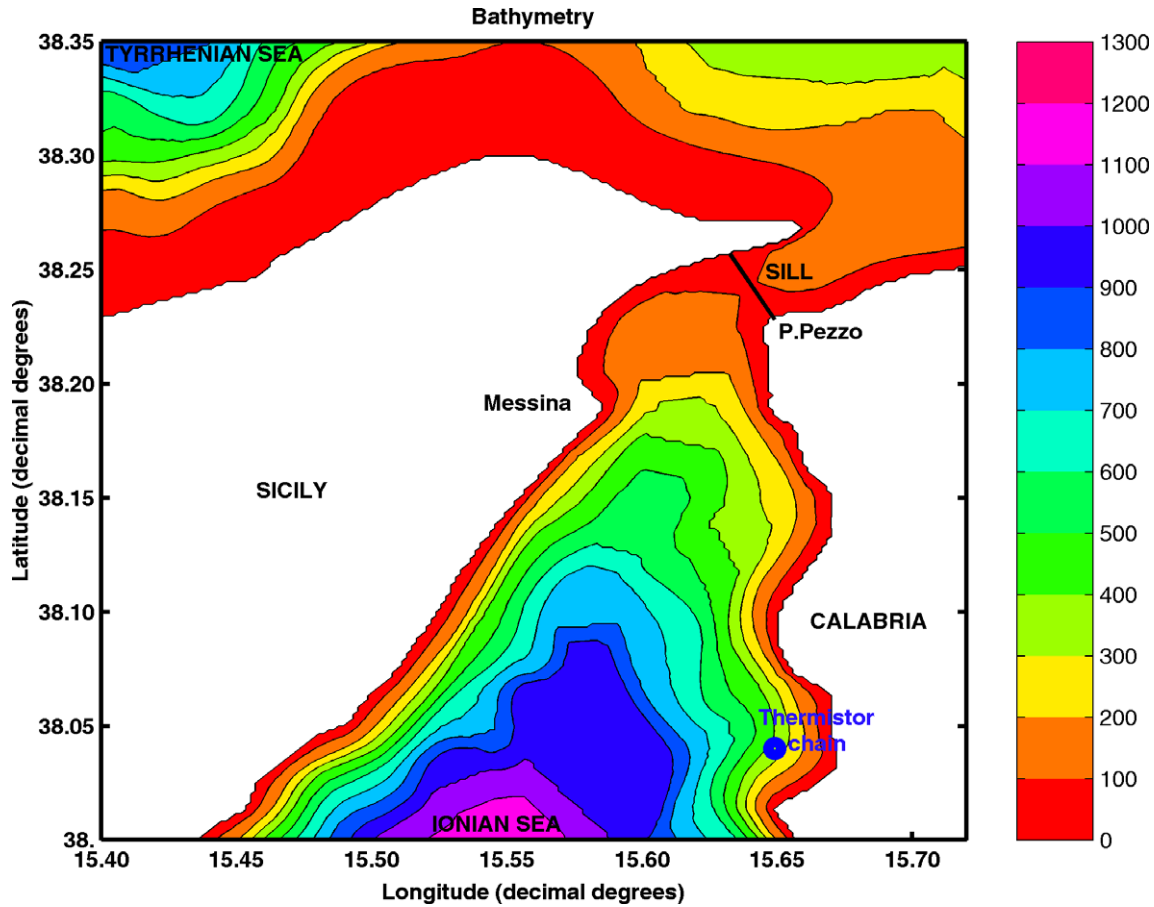


Fig. 1. Bathymetry of the Strait of Messina. The blue point shows the thermistor string position.

oscillate almost in opposition, thus leading to a sea surface slope of $1\text{--}2\text{ cm km}^{-1}$ generating strong currents (Mosetti, 1988) as high as 3 m s^{-1} in the sill region during spring tides (Bignami and Salusti, 1990).

Strong barotropic tidal flow, steep bathymetry, and stably stratified environment are the three required ingredients for internal wave generation (Zeilon, 1912). The generation process was demonstrated analytically in Baines (1973, 1982). Several hydrodynamic modelling studies have been done and have showed that a tidal flow going over steep topography creates an interfacial depression of the pycnocline that generates an internal bore (Del Ricco, 1982; Mosetti, 1988; Lamb, 1994; Brandt et al., 1997; Warn Varnas et al., 2003, 2005, 2007). Concerning the Strait of Messina, the heavier Levantine Intermediate Water crosses the sill during *rema montante*. The pycnocline is thus lifted at the sill, and then depressed in the northern basin. The depression generates a southwards and a northwards propagating bore. The northwards travelling bore keeps propagating in the Tyrrhenian Sea whereas the southwards propagating bore is stopped by the sill. When the semi-diurnal tide reverses to *rema scendente*, the southwards propagating internal depression undergoes a hydraulic jump over the sill and into the southern basin where it propagates away from the sill. As it propagates, nonlinear effects steepen its leading edge until it disintegrates into a series of “train” of interfacial nonlinear short internal waves. This disintegration is due to effects of frequency and amplitude dispersions, as well described in Warn Varnas et al. (2007). Internal waves in the Strait of Messina are characterized by a propagation speed between 0.80 and 1.15 m s^{-1} , with oscillations of temperature up to $2\text{ }^{\circ}\text{C}$ amplitude. When the train is well formed, 4–10 internal solitary waves per train

can be observed with periods ranging from 8 to 30 min, covering an average total duration of about 2 h (Alpers and Salusti, 1983; Casagrande et al., 2009).

In this paper, we present an original way of detecting and characterizing internal waves through empirical orthogonal function (EOF) decomposition applied to *in situ* data from the COACH06 cruise (late October – beginning of November 2006). After a brief presentation of the data set and the EOF analysis theory, the computed expansion coefficients are analyzed by studying the behaviour of their time derivatives, and the corresponding scatter diagrams. In the presence of an internal wave, a characteristic feature, also giving information about the wave width, appears.

2. Experimental data

For this study, the measurements came from one thermistor chain bottom-moored south of the sill (Fig. 1), at location ($15^{\circ}38'57''\text{E}$, $38^{\circ}02'24''\text{N}$), from 4 November 16:48 UTC to 7 November 07:12 UTC, with a 1-min temporal resolution which allows clear observations of internal solitary wave events. The chain consisted of 10 sensors ranging from 14 to 128 m depth, providing a vertical resolution of about 10 m. Fig. 2 shows the density computed from the temperature measurement of the thermistor string using the UNESCO equation of state (salinity was considered constant with a value of 38.10 psu).

The pycnocline depth stands around 95 m for the first day and half, and rises slowly to a 60 m depth after 6 November. Five internal solitary wave train events can be identified on the whole period; they occur every half day, corresponding to the tidal period. The maximum amplitudes of the internal waves range from 40 to

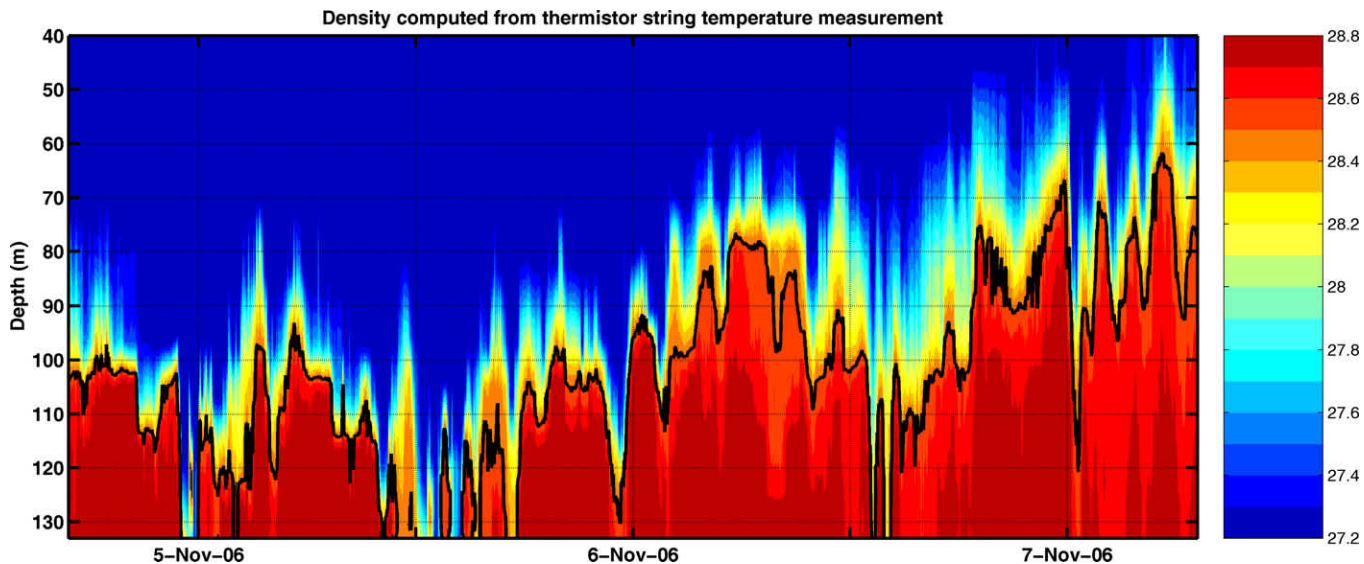


Fig. 2. Density computed from thermistor string measurements from 4 November 2006 16:48 UTC to 7 November 2006 07:12 UTC. The 28.5 density contour (corresponding to a temperature of 16 °C) is plotted to underline the density variability due to occurrence of internal waves. Density units are “sigma-t”.

50 m. The trains have two to four internal solitary waves. The first and second waves are very neat in the data. On average, it was observed that the internal wave trains appear on the thermistor string data 6–6.5 h after the tide reversal from *rema montante* to *rema scendente*. Considering the hypothesis made by Alpers and Salusti (1983) that, for southwards propagating internal solitary waves, the internal bores are generated at slack waters when the flow reverses from north to south, the average speed of the internal waves train was estimated between 1.03 and 1.15 m s⁻¹.

3. EOF analysis

An empirical orthogonal function (EOF) decomposition of the time series of density was carried out to gain more information on the internal wave structure. This decomposition determines the main spatial patterns of variability as well as their variation in time and gives a measure of importance of each pattern (Emery and Thomson, 1997). Each EOF mode represents a standing oscillation pattern (Preisendorfer, 1988). The projection of the data onto the EOF modes gives an estimate of how the pattern oscillates in time. These projections are called principal component time series or expansion/projection coefficients of the EOFs.

In our study, the EOF analysis was applied on the vertical to the density anomaly obtained from the thermistor string measurement, so that the density $\sigma(z, t)$ could be written as:

$$\sigma(z, t) = \langle \sigma(z) \rangle + \sum_{n=1}^M \alpha_n(t) \phi_n(z) \quad (1)$$

where $\langle \sigma(z) \rangle$ is the time-averaged vertical density profile, M is the number of considered EOF modes, $\alpha_n(t)$ is the amplitude (or ‘expansion coefficient’) of the n th orthogonal mode at time t and $\phi_n(z)$ the n th EOF. This equation says that the time variation of the dependent scalar variable $\sigma(z, t)$ at each depth results from the linear combination of M spatial functions ϕ_n , whose amplitudes are weighted by M time-dependent expansion coefficients $\alpha_n(t)$. The weights $\alpha_n(t)$ tell how the spatial modes ϕ_n vary with time. As there are many terminologies for EOF analysis, we insist on the fact that the use of “EOF”, or EOF mode, refers to the spatial vertical pattern ϕ_n , and that “expansion coefficient”, or projection coefficient, refers to the temporal patterns or weights $\alpha_n(t)$.

With the inherent efficiency of this statistical description, a very few empirical modes are needed to describe the fundamental variability in a very large data set. Here the first mode represents over 95% of the variance, the second mode drops to 4.5%, the others are negligible. So only the first two modes, representing 99.5% of the variance, are taken into account, and represented in Fig. 3 with their respective expansion coefficients. The two vertical modes are very clean and smooth. The amplitude of the first EOF does not change sign over the water column, it is maximum at a depth of 90 m. Therefore, all the isopycnals oscillate in the same direction (Vázquez et al., 2006) with maximum displacement at 90 m. It represents the vertical displacement of the pycnocline; the oscillation, where the EOF is not null, can be felt between 45 and 130 m depth, which corresponds well to what is observed on Fig. 2. The second EOF has two extrema, as a consequence of the orthogonality constraint, and changes sign close to the first EOF maximum depth. This indicates that isopycnals are moving in opposite directions above and below the pycnocline (Vázquez et al., 2006). It represents a change in the thickness of the pycnocline, and consequently a modification of the vertical density gradient. Interpreting EOFs must always be done cautiously as empirical modes do not necessarily correspond to physical modes (Dommenges and Latif, 2002). The physical mode base functions have increasing number of sign changes as the vertical mode number increases. The first mode does not change sign. The second mode changes sign once. This is similar to first and second EOF functions. They both track vertical variability but their equivalence or non equivalence remains to be determined.

Looking now at the expansion coefficients on Fig. 3 bottom, it can be observed that their behaviour is related to internal wave occurrences, both coefficients assuming much larger absolute values during internal wave events. It can also be noticed how well the first expansion coefficient agrees with the pycnocline oscillation of Fig. 2, once again confirming that the first mode corresponds to the vertical displacement of the pycnocline.

As most of the variance was contained in the first two spatial modes and as the expansion coefficients have a similar behaviour, we looked at the scatter diagram formed by plotting the first expansion coefficient α_1 versus the second expansion coefficient α_2 . The result reveals a crescent shaped distribution (Fig. 4) meaning that both expansion coefficients are dynamically linked (Casagrande et al. 2008). We have reminded this result here as when it was first published in Casagrande et al. (2009), a lot of questions

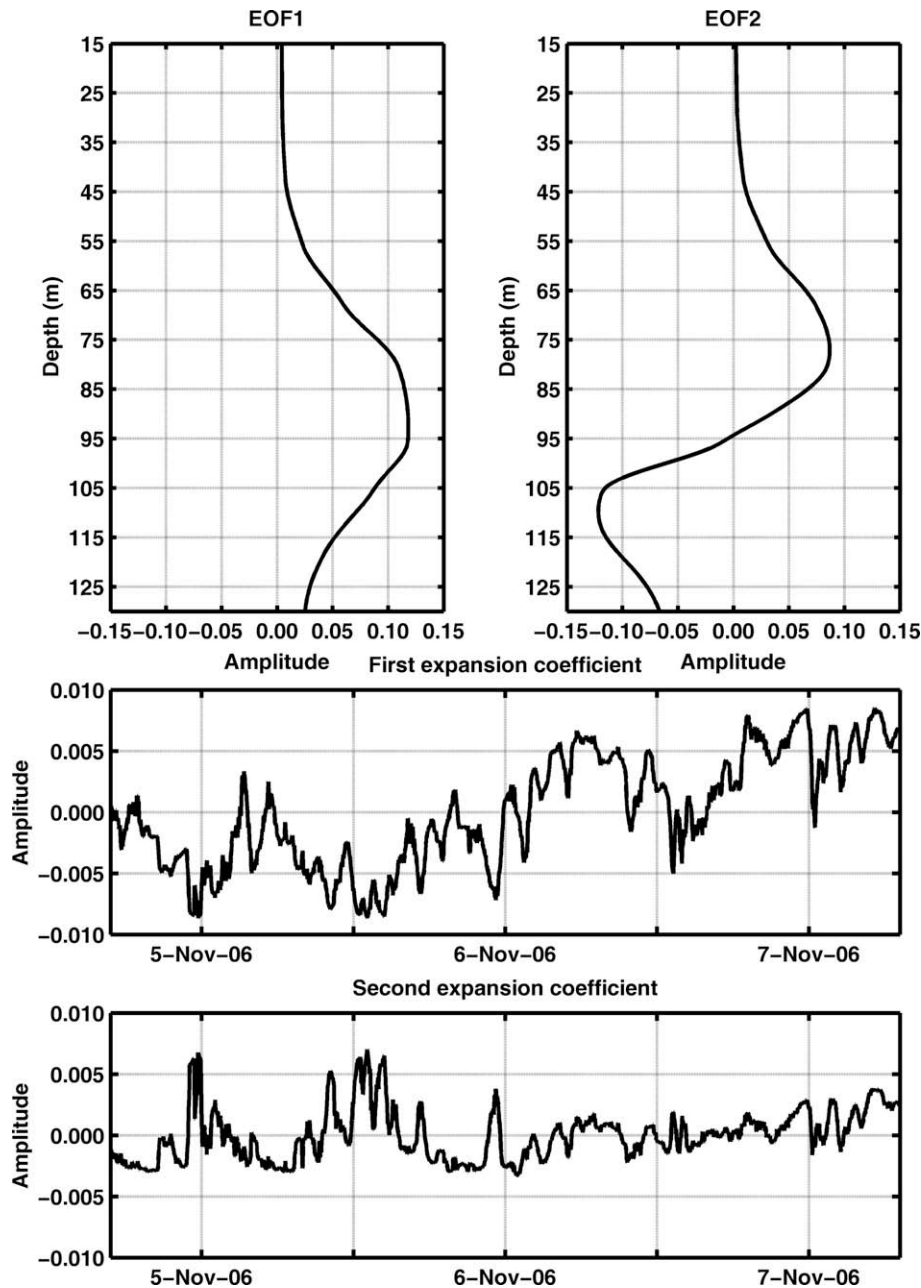


Fig. 3. Top, amplitude of first two EOFs ϕ_1 and ϕ_2 calculated from the thermistor string density. Only the first two EOFs are represented as they give over 99% of the variance (95% and 4.5%). Bottom, expansion coefficients for the first two EOF modes. The first expansion coefficient clearly represents the vertical oscillation of the pycnocline in time (compare with density contour 28.5 on Fig. 2). Both coefficients have stronger (absolute) values during internal wave events.

arose from the reviewers and the scientific community. EOFs are built under some orthogonal constraints: (1) the EOF modes $\phi_i(z)$ are orthogonal in space meaning that there is no correlation between any two EOFs ($\phi_i \cdot \phi_j = \delta_{ij}$) and (2) the expansion coefficient time series $\alpha_i(t)$ are orthogonal in time meaning that there is no simultaneous temporal correlation between any two expansion coefficients ($\alpha_i \cdot \alpha_j = \delta_{ij}$). These two constraints were checked and respected for the first two EOF modes considered here: $\phi_1 \phi_2 = 0$ and $\alpha_1 \alpha_2 = 0$. The scatter diagram of the expansion coefficients having a specific shape is not in contradiction with the orthogonality constraint, it only highlights a dynamical interaction between these two modes illustrating that the vertical oscillation of the pycnocline during an internal wave event is related to the modification of its gradient.

Two regimes can be distinguished in Fig. 4. In the centre of the distribution where the cloud of points is thick and dense, α_1 takes small values meaning a weak variation of the pycnocline depth. α_2 is negative. This corresponds to density profiles with a pycnocline depth close to the average and a gradient typical of a well stratified water column (Casagrande et al., 2008). This regime represents a “rest regime” with no internal wave events. Looking now at the “branches” of the “crescent”, one can see how both coefficients increase in absolute values in a correlated way. This regime represents the internal wave dynamics. More details are available in Casagrande et al. (2009). This crescent shape scatter diagram was confirmed by numerical simulations (Fig. 4) from the fully non-hydrostatic 2.5D Lamb model (1994) described in Casagrande et al. (2008, 2009).

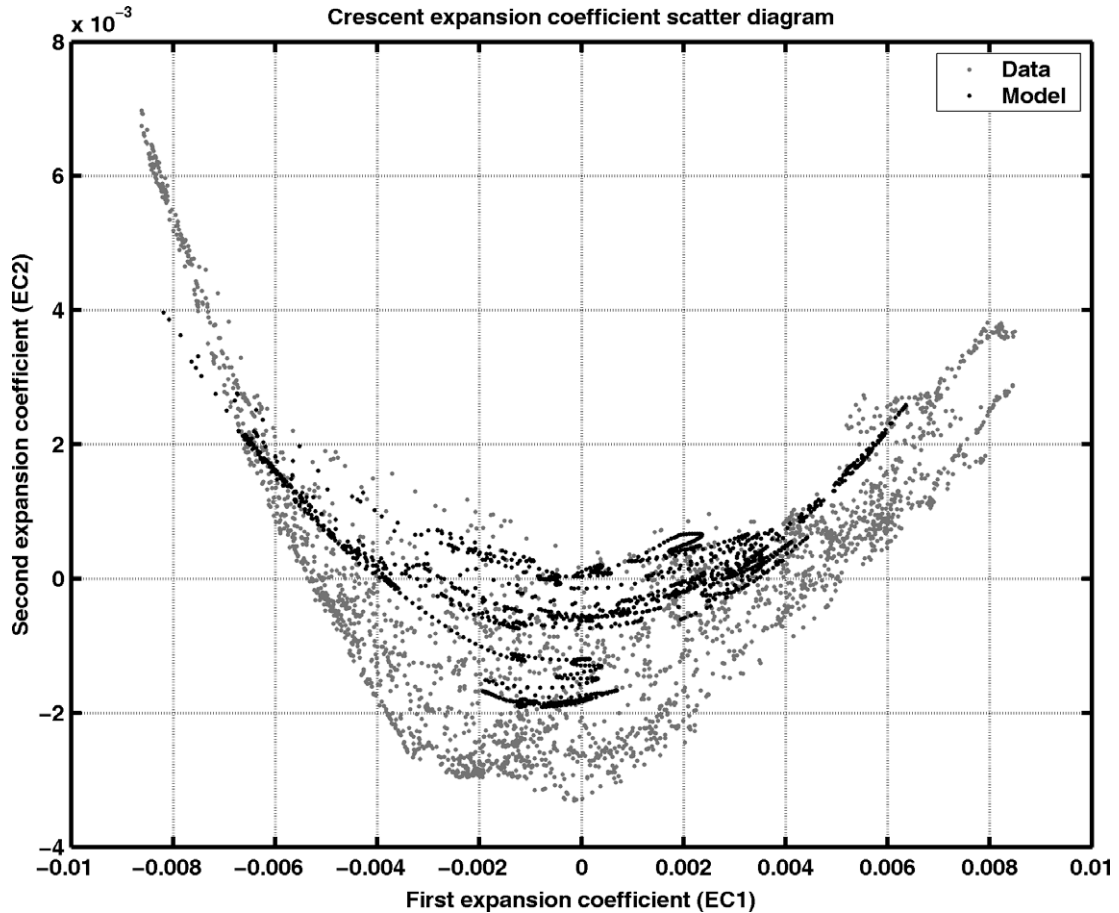


Fig. 4. Expansion coefficient scatter diagram for the thermistor string data (grey) and the Lamb model (1994) output (black). The scatter diagram is obtained by plotting the first two expansion coefficients α_1 and α_2 versus one another. The “crescent shape” of the scatter diagram shows that the two main EOF expansion coefficients are dynamically linked in the presence of internal waves. The “middle” of the cloud of points represents the interval between two internal wave events when the profile is close to its mean position. The asymptotic behaviour of the cloud of points for high values of the expansion coefficients is representative of internal wave events.

4. Results

As the observed crescent scatter diagram is representative of internal wave dynamics and in order to see how the diagram of the expansion coefficients is described in the presence of an internal wave event, the time derivatives of the expansion coefficients, called here ‘changing rates’ (CR), are computed: $CR_1 = d\alpha_1/dt$ and $CR_2 = d\alpha_2/dt$. These changing rates represent the variation in time of the expansion coefficients. As the expansion coefficients have bigger absolute values during internal wave occurrences, the changing rates should vary accordingly. They are plotted in Fig. 5 for an internal wave train observed in the thermistor string data and for an internal wave train generated by the Lamb model (1994). In both cases, the changing rates have a particular behaviour that consists in a double oscillation for each encountered wave in the internal wave train. Let us consider three areas in a wave: the front of the wave (first half of the wave corresponding to the deepening of the isopycnals), the maximum of the wave (deepest point of the wave and maximum amplitude), and the rear of the wave. The changing rates are close to zero in the absence of internal waves. When a wave appears, the changing rates both increase considering their absolute values: for the front of the wave, CR_2 describes a positive oscillation while CR_1 describes a negative oscillation; when the wave reaches its maximum amplitude, CR_1 and CR_2 are both back to zero; eventually at the rear of the wave, CR_1 and CR_2 evolve again as two opposite oscillations but this time positive for CR_1 and negative for CR_2 . The first phase corresponds to the

depression of the pycnocline, the pycnocline deepens (CR_1 is negative) and the gradient in the pycnocline becomes stronger as the pycnocline becomes thinner with the steepening of the front of the wave (CR_2 is positive). When the wave reaches its maximum depth, the changing rates are equal to zero as a consequence of null derivative for extrema. In the last phase, the pycnocline returns to its average shallower depth (CR_1 is positive) and its thickness increases to return to an average stratification (CR_2 is negative). This is what we called the *double oscillation* pattern; it can be identified for each wave of the data wave train and the modelled wave train of Fig. 5. To sum up, a positive CR_1 means a shallowing of the pycnocline and a negative CR_1 means a deepening of the pycnocline. A positive CR_2 means a thinner pycnocline and a stronger gradient and a negative CR_2 means a thicker pycnocline and a weaker gradient (average stratification).

This methodology can then be applied to detect the internal waves in the water column. This is illustrated for another internal wave train extracted from the thermistor string data in Fig. 6. The first two depressions correspond to internal waves with the particular changing rate double oscillation feature. However, the third depression, which is visually alike the previous ones, has not the proper evolution of the changing rates and is not to be assimilated to an internal wave. The considered internal wave train contains thus two waves and not three. This result is interesting as internal wave trains are not always straightforward to detect in data. In the thermistor string measurement of Fig. 2, internal wave dynamics are neatly illustrated, but it is hard to tell if all oscillations of the

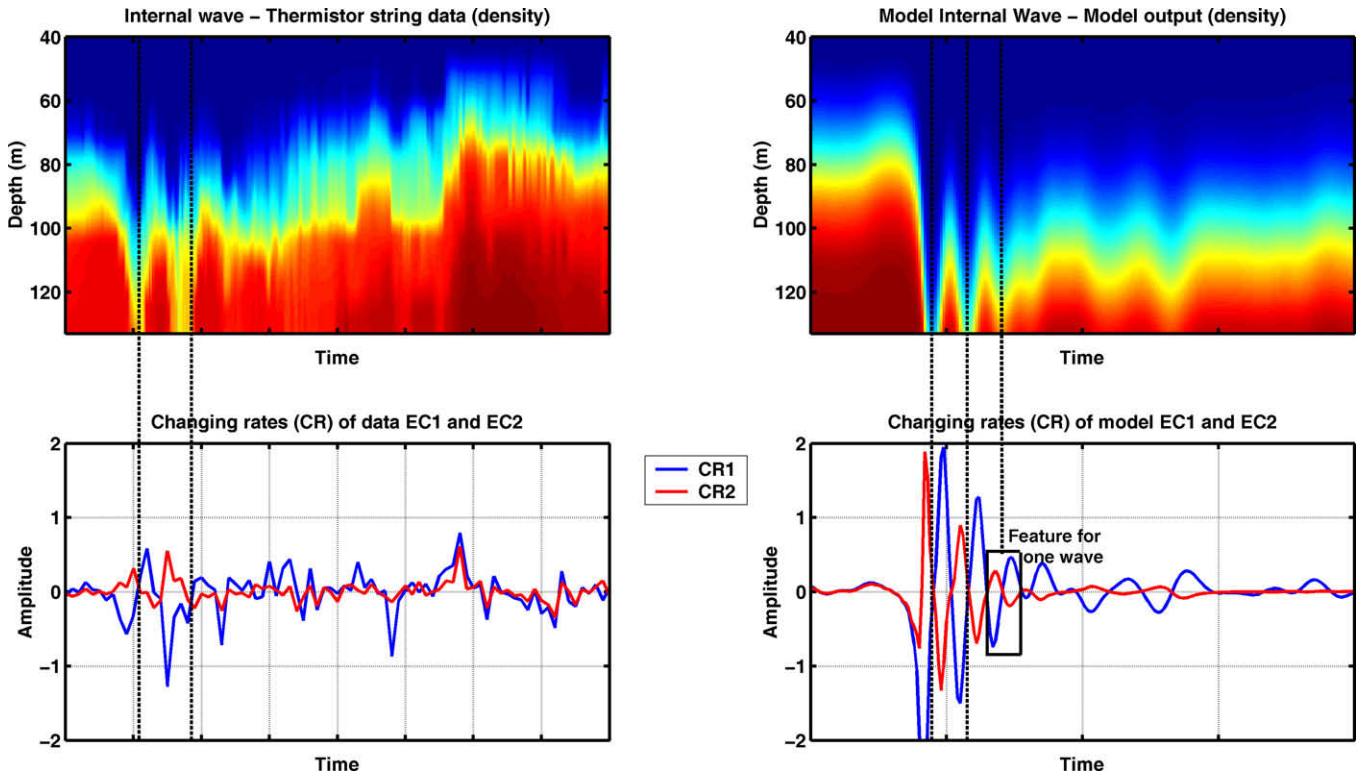


Fig. 5. Bottom, changing rates (time derivative of the expansion coefficients) plotted for two internal wave trains (top) extracted from the thermistor string (left) and from the model (right). Both changing rates have a particular behaviour for an internal wave. They both increase but with opposite sign, on the front of the wave. At the deepest of the wave, they are both back to zero to evolve in opposite ways, once again with opposite signs. This is the *double oscillation* pattern.

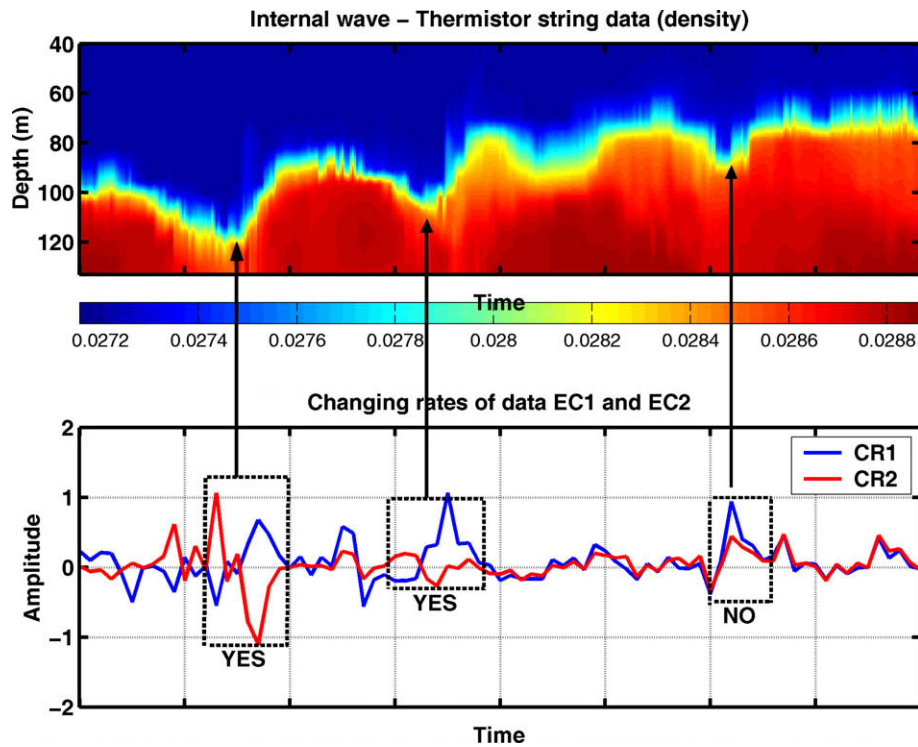


Fig. 6. Internal waves, to be or not to be? Same as Fig. 5 in order to illustrate that the changing rates behaviour can be used as internal wave detector. The first two depressions correspond to internal waves with the particular changing rate feature observed and described before. However the third depression, that is visually alike the previous ones, has not the proper corresponding changing rate behaviour and is not to be considered as an internal wave. The considered internal wave train contains thus two waves and not three.

pycnocline are proper internal waves. With this method, oscillations are easily identified as internal waves or not. The double oscillation also gives an important information on the width of the wave: when estimating the width of a wave from the data series, an inaccuracy can lie in the estimation of the ‘beginning’ and the ‘end’ of the wave whereas the width of the double oscillation is easily measurable (dotted squares in Figs. 5 and 6). Even though it is not concerning the same entity, it is interesting to notice that these double oscillations also appear in Vázquez et al. (2006) on the time series of the modelled vertical velocity amplitude considered at the depth where their first two EOF modes are maximum (unfortunately, the double oscillation does not appear in the *in situ* ADP measured vertical velocities). The link between these two features is not straightforward, but the ‘coincidence’ has enough interest to be mentioned.

Finally, as done for the expansion coefficients, the scatter plot of the changing rates one versus another is plotted (Fig. 7). This scatter plot puts on a butterfly shape, named *farfalla* scatter plot (as this study was partly made in Italy). Helping our analysis with the neat scatter plot of the model changing rates, it is seen that the scatter diagram is divided in four zones limited by the two lines $CR_2 = CR_1$ and $CR_2 = -CR_1$. The two quarters available in the scatter plot correspond to $|CR_2| \leq |CR_1|$. The two other quarters are strictly forbidden, at least for the scatter plot issued from the model. It means that the variation of the first changing rate is always stronger than that of the second one. It corresponds to what is observed when plotting the changing rates versus time in Fig. 5. This rule applies very well to the changing rates of the model expansion coefficients whereas there are exceptions for the changing rates of the data expansion coefficients (e.g. first wave in Fig. 6). In the presence of an internal wave, the positive extrema of CR_2 corresponds to the negative extrema of CR_1 and vice versa. When there is no internal wave, CR_2 varies very slightly around 0 while CR_1 undergoes slightly bigger oscillations thus always respecting

the latter rule. Physically, it means that a minimum vertical translation of the pycnocline is needed to impact on the slope of the gradient and lead to internal wave generation: small oscillations of CR_1 , and consequently oscillations of the pycnocline, are observed after the internal wave train in Fig. 5 for the data and for the model, but they do not generate a change in CR_2 , which means no modification in the pycnocline thickness, and are then not considered as internal waves. Once again, this highlights the dynamical link between the two EOF modes.

5. Summary and conclusions

The Strait of Messina with its shallow sill and strong tidal currents leading to strong interfacial depressions is an important place of internal bore generation and internal solitary wave occurrence. As internal waves are hard to model with classical 3D ocean models (need of tidal dynamics, high resolution, non hydrostatic), alternative ways to detect and characterize these dynamical processes were looked at, in particular by using statistical analysis. Our study is based on empirical orthogonal function analysis (EOF) and uses only the first two resulting EOF modes and their corresponding expansion coefficients. A first study (Casagrande et al., 2009) had shown that both expansion coefficients were dynamically linked when plotting them one versus another in a scatter plot. In order to develop this result for more efficient applications, the time derivatives, named *changing rates*, of the expansion coefficients were computed and studied. For each occurrence of internal wave, these changing rates have a typical behaviour we called *double oscillation*. The dynamics of internal waves are neatly visible in time series, but it is sometimes not straightforward to identify neatly each wave of an internal wave train for example. The double oscillation is then a good indicator of the presence of internal waves. Two figures can be extracted from this feature: the number of double oscillations gives the number of waves per internal wave

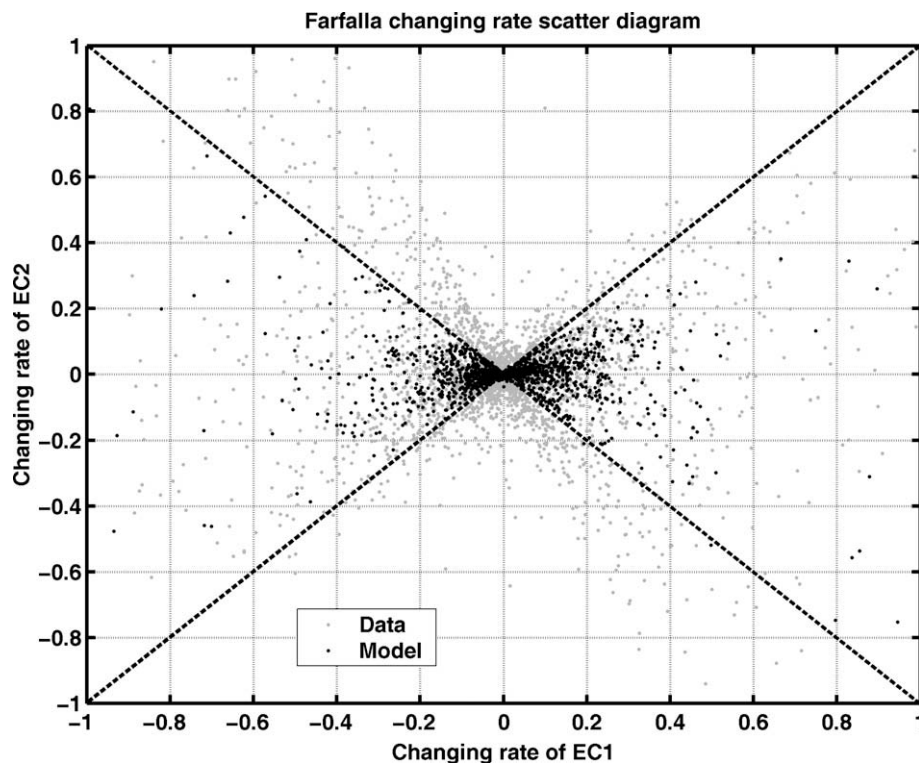


Fig. 7. As done for the expansion coefficients, the scatter diagram of the changing rates versus one another is plotted for the thermistor string data (grey) and the Lamb model (1994) output (black). This scatter plot has a particular shape resembling a butterfly or ‘farfalla’ in Italian. The two dashed lines represent $CR_2 = CR_1$ and $CR_2 = -CR_1$.

train, and their widths correspond to the widths of the considered waves, which are usually difficult to determine accurately from data time series. This methodology works well as the dynamics in the Strait of Messina are essentially driven by tides and constrained in a small area, thus leading to a very few overwhelming EOF modes. Yet these statistical approaches for studying internal waves are added-value to detect and characterize a phenomenon which is usually difficult to model.

Acknowledgments

This study was carried out thanks to the Joint Research Program (JRP) COACH between NURC, SHOM and NRL. Part of this work was supported by the Office of Naval Research under PE 62435N with technical management provided by the Naval Research Laboratory. We are very thankful to Emanuel Coelho and Jim Richman for their useful comments on the EOF analysis. We thank as well the anonymous reviewer for having tried out our methodology on a set of data in a different area (and it seems to have worked out!).

References

- Alpers, W., Salusti, E., 1983. Scylla and Charybdis observed from space. *Journal of Geophysical Research* 88 (C3), 1800–1808.
- Baines, P., 1973. The generation of internal tides by flat-bump topography. *Deep Sea Research* 20, 179–205.
- Baines, P., 1982. On internal tide generation models. *Deep Sea Research* 29, 307–338.
- Bignami, F., Salusti, E., 1990. Tidal currents and transient phenomena in the Strait of Messina: a review. *The Physical Oceanography of Sea Straits* 95, 124.
- Brandt, P., Rubino, A., Alpers, W., Backhaus, J.O., 1997. Internal waves in the Strait of Messina studied by a numerical model and synthetic aperture radar images from ERS ½ satellites. *Journal of Physical Oceanography* 27 (5), 648–663.
- Casagrande, G., Folégot, T., Stéphan, Y., Warn Varnas, A., 2008. Characterization and mode coupling of internal waves in the Strait of Messina. Internal NURC report NURC-FR-2008-029, 52.
- Casagrande, G., Warn Varnas, A., Stéphan, Y., Folégot, T., in press. Genesis of the coupling of internal wave modes in the Strait of Messina. *Journal of Marine Systems*. doi:10.1016/j.jmarsys.2009.01.017.
- Defant, A., 1940. Scilla e Carridi e le correnti di marea nello Stretto di Messina. *Geophysica Pura e Applicata* 2, 93–112.
- Defant, A., 1961. Tides in the Mediterranean and adjacent seas. Observations and discussion. Chapter 12. *Physical Oceanography* 1, Pergamon Press, 364–456.
- Del Ricco, R., 1982. Numerical model of the internal calculation of a strait under the influence of the tides, and its application to the Messina Strait. *Il Nuovo Cimento* 5 (C1), 21–45.
- Dommenget, D., Latif, M., 2002. A cautionary note on the interpretation of EOF. *Journal of Climate* 15 (2), 216–225.
- Emery, W., Thomson, R., 1997. *Data Analysis Methods in Physical Oceanography*. Elsevier, Amsterdam, Netherlands, 634.
- Lamb, K., 1994. Numerical experiments of internal wave generation by strong tidal flow across a finite amplitude bank edge. *Journal of Geophysical Research* 99 (C1), 843–864.
- Mosetti, F., 1988. Some news on the currents in the Strait of Messina. *Bolletino di Oceanologia Teorica e Applicata* VI (3), 119–201.
- Preisendorfer, R.W., 1988. *Principal Component Analysis in Meteorology and Oceanography*. Elsevier, p. 425.
- Vázquez, A., Stashchuk, N., Vlasenko, V., Bruno, M., Izquierdo, A., Gallacher, P.C., 2006. Evidence of multimodal structure of the baroclinic tide in the Strait of Gibraltar. *Geophysical Research Letters* (33), 6.
- Warn Varnas, A., Chin-Bing, S.A., King, D.B., Hallock, Z., Hawkins, J.A., 2003. Ocean-acoustic solitary wave studies and predictions. *Surveys in Geophysics* 24, 39–79.
- Warn Varnas, A., Hawkins, J.A., Lamb, K.G., Texeira, M., 2005. Yellow Sea ocean-acoustic solitary wave modelling studies. *Journal of Geophysical Research* 110 (C08).
- Warn Varnas, A., Hawkins, J., Smolarkiewicz, P.K., Chin-Bing, S.A., King, D., Hallock, Z., 2007. Solitary waves effects north of Strait of Messina. *Ocean Modelling* 18, 97–121.
- Zeilon, N., 1912. On the tidal boundary waves and related hydrodynamical problems. *Kungl Svenska Vetenskapsakademiens Handlingar* 47 (4), 46.